

The elastic stability, bifurcation and ideal strength of gold under hydrostatic stress: an *ab initio* calculation

Hao Wang^{1,2} and Mo Li^{1,3}

¹ School of Materials Science and Engineering, Georgia Institute of Technology, Atlanta, GA 30332, USA

² School of Physics, Georgia Institute of Technology, Atlanta, GA 30332, USA

E-mail: mo.li@mse.gatech.edu

Received 22 August 2009, in final form 26 September 2009

Published 23 October 2009

Online at stacks.iop.org/JPhysCM/21/455401

Abstract

In this paper, we employ an *ab initio* density functional theory calculation to investigate the elastic stability of face-centered cubic Au under hydrostatic deformation. We identify the elastic stiffness constant B_{ijkl} as the coefficient in the stress–strain relation for an arbitrary deformed state, and use it to test the stability condition. We show that this criterion bears the same physics as that proposed earlier by Frenkel and Orowan and agrees with the Born–Hill criterion. The results from those two approaches agree well with each other. We show that the stability limit, or instability, of the perfect Au crystal under hydrostatic expansion is not associated with the bulk stiffness modulus as predicted in the previous work; rather it is caused by a shear instability associated with the vanishing rhombohedral shear stiffness modulus. The deviation of the deformation mode from the primary hydrostatic loading path signals a bifurcation or symmetry breaking in the ideal crystal. The corresponding ideal hydrostatic strength for Au is 19.2 GPa at the Lagrangian expansion strain of ~ 0.06 . In the case of compression, Au remains stable over the entire pressure range in our calculation.

1. Introduction

The strength of crystalline materials is determined in general by the nucleation and motion of dislocations or microcracks. If there are no such defects, the materials would fail at the limit of so-called stability, including elastic and phonon stability. The stress at which this is achieved is called the ideal strength. It is of great interest to investigate the elastic behavior of a perfect crystal under loading because the path leading toward the instability is related to not only the ideal strength but also the atomic mechanisms of the defect formation. Such information is also very useful in the analysis of the structural response of solids, ranging from polymorphism to amorphization to fracture. Moreover, the ideal strength is connected to the strength and defect formation in nanostructured materials currently being developed, as shown in recent nanoindentation experiments where the onset of yielding on the nanoscale is suggested to be related to homogeneous nucleation of

dislocations in the small volume under the nanoindenter where stresses approach the ideal strength [1].

The elastic stability limit is formulated traditionally following Born's original idea [2, 3] that a crystal should remain stable when the change of the elastic energy with respect to the spontaneous strain exhibits convexity; otherwise, instability would occur consequentially. The condition of convexity leads to the stability criteria in the form of a set of relations involving elastic constants appropriate to the crystal symmetry. Born's theory is, however, formulated for systems without an external load. For systems under an external load, it was shown [4–14] that the elastic stiffness coefficients B_{ijkl} (equation (6) below) rather than elastic constants C_{ijkl} should be used in formulating the stability criteria. The onset modes at the instability derived from the stability criteria were tested for many crystalline systems using various approaches employing empirical or semi-empirical inter-atomic potentials such as the Lennard-Jones potential [9], the Morse potential [14] or EAM potentials [11]. It is known that these inter-atomic interactions are obtained by fitting the parameters predominantly with the

³ Author to whom any correspondence should be addressed.

equilibrium properties of the material studied (i.e., under zero or infinitesimal deformation). It is, therefore, doubtful that one should apply those potentials obtained this way to simulate the materials under finite loading and still expect to obtain reliable results. *Ab initio* electronic structure calculations, on the other hand, have been performed for variously strained structures and are shown to give the ideal strength of materials without resorting to doubtful extrapolations. Given recent advances in quantum theoretical methods and computers, it is possible to calculate the elastic limits with considerable accuracy, including both the theoretical stress and the detailed nature of the atomic rearrangements as the elastic limit is approached. For instance, Senoo *et al* discussed the elastic deformation due to [100] loading of Al using the pseudopotential method [15]. Esposito *et al* dealt with the tensile strength of fcc Cu under uniaxial deformation on the basis of the *ab initio* potential, augmented-spherical-wave (ASW), and KKR methods [16]. Friak *et al* did extensive investigation of the ideal strength of bcc iron under hydrostatic pressure, and due to [001], [111] uniaxial tension [17]. Li and Wang studied the ideal tensile strength of Al [18]. Cerny *et al* worked on the tensile strength of Cu [19]. Cerny *et al* also tested the elastic stability of some magnetic crystals under hydrostatic pressure [20].

The stability criterion based on the elastic stiffness constants [11–13] certainly provides a convenient and powerful recipe for measuring the stability limit. As was done in these previous works, one first calculates the elastic constants and then constructs the elastic stiffness coefficients as a function of the stress applied to a system, which is usually under some specific load such as hydrostatic, uniaxial tensile or compressive, or shear strain. One then obtains the stability limit at the strain where a principal minor of the elastic stiffness constant matrix first becomes non-positive, or $\det|B_{ijkl}| = 0$. While along some simple loading paths such as uniaxial tension and compression the stability limit is found to relate to some shear strain modes [18, 19], under hydrostatic loading it is observed that the stability is dominated by the bulk stiffness coefficient that corresponds to void formation under expansion [11]. The possibility of bifurcations from the primary loading path or mode before the stability limit is approached was seldom observed in the case of hydrostatic loading. As we show below, the stability limit of Au under a hydrostatic load is actually caused by shear not by volume instability as shown in the earlier work [11]. As considered in the earlier studies, noticeably by Born [2, 3] and Hill [4–8], some perturbations, fluctuations, as well as sample loading conditions would make the deformation path stray from the primary loading path, causing the measured stability limit to be different from that intended originally. As we show here, this phenomenon, which is called ‘stability bifurcation’, plays an important role in determining the global stability of a crystal lattice.

In this paper, we present a direct investigation, using density functional theory (DFT), of the elasticity, the stress–strain relation, the stability, and the ideal strength of fcc metal Au under hydrostatic stress. Au is special in its structural stability, known experimentally to have no polymorphism under hydrostatic compression, so its original symmetry is

preserved on the primary loading path under hydrostatic stress before the instability limit, yet to be identified. Thus it provides a simple test case for a stability study. Therefore, the possible bifurcation along paths different from the primary loading path can be addressed relatively clearly. The additional motivation is drawn from the earlier studies made by Wang *et al* on Au [11]; they performed molecular dynamics (MD) simulation using classical EAM potentials. As shown below, our results are different from theirs in that the stability limit of Au under hydrostatic expansion is dominated by shear instability, not by volumetric or bulk modulus instability. This unusual finding is a direct manifestation of the stability bifurcation.

This paper is organized as follows. The stability criterion of a crystal solid is presented briefly in section 2. In this section, we review the formulation of the stress, elastic stiffness coefficients, elastic stiffness moduli, and stability criteria. In particular, we shall give a new interpretation of the stability criterion based on the elastic stiffness coefficients from the stress–strain relation in any deformed state. In section 3, we introduce our calculation models and methods and the *ab initio* DFT method. In section 4, we show our results. In section 5, we discuss our results and make comparisons with some related previous work. Finally, we will draw conclusions from this work.

2. The stability criterion of crystal solids

For a solid body subject to an external loading, the configuration of a material point in the system after elastic deformation is represented as $Y = Y(X)$, where X is the initial configuration in the equilibrium state. The deformation gradient is defined by

$$J_{ij} = \frac{\partial Y_i}{\partial X_j}, \quad (1)$$

where $i, j = 1, 2, 3$ are the indices of the Cartesian coordinates. Then the Lagrangian strain tensor is defined as

$$\eta = \frac{1}{2}(J^T J - I), \quad (2)$$

where I is the unit matrix. The internal energy is related to the Lagrangian strain through Taylor series expansion in terms of the strain tensor [21],

$$U(X, \eta_{ij}) = U(X, 0) + V \sum_{ij} \sigma_{ij} \eta_{ij} + (1/2!)V \sum_{ijkl} C_{ijkl} \eta_{ij} \eta_{kl} + \dots, \quad (3)$$

where

$$\sigma_{ij} = V^{-1}(\partial U / \partial \eta_{ij})_{\eta=0} \quad (4)$$

$$C_{ijkl} = V^{-1}(\partial^2 U / \partial \eta_{ij} \partial \eta_{kl})_{\eta=0}, \quad (5)$$

and V is the volume in the configuration X . If the system is under load, the stability criterion depends on the elastic stiffness coefficients, instead of the elastic constants as defined in equation (5) in Born’s theoretical framework. The definition of the elastic stiffness coefficients is as follows:

$$B_{ijkl} = C_{ijkl} + (1/2)(\delta_{ik} \tau_{jl} + \delta_{jk} \tau_{il} + \delta_{il} \tau_{jk} + \delta_{jl} \tau_{ik} - 2\delta_{kl} \tau_{ij}), \quad (6)$$

where τ_{ij} is the external stress, which is equal to the internal stress σ_{ij} (equation (4)) if the system remains in mechanical equilibrium. This derivation of B_{ijkl} is from the premise proposed by Hill and Milstein [4–8] that a solid can only be in a stable state when the change of the internal energy δU is larger than the external work δW done to the system, or $\delta U - \delta W > 0$.

Here we give another, and physically more transparent, definition of the elastic stiffness coefficients B_{ijkl} and the new interpretation of the stability criterion, which is based on the stress–strain relations in any deformed state. If a material in configuration X under stress $\sigma_{ij}(X)$ is stable, then after a given small perturbation, i.e. with a small strain η_X^Y , the system will move to a new state Y with a corresponding stress $\sigma_{ij}(Y)$. The two stresses are related by a linear proportional coefficient of stress versus strain between the two states (X and Y) of the stressed system as shown by Wallace [21],

$$\sigma_{ij}(Y) = \sigma_{ij}(X) + B_{ijkl}(\eta_X^Y)_{kl} + O[(\eta_X^Y)^2]. \quad (7a)$$

If the material in the state X is stable, then the increment of the stress $\delta\sigma_{ij} = \sigma_{ij}(Y) - \sigma_{ij}(X)$ must remain positive to the first order in the perturbative strain η_X^Y , or

$$\delta\sigma_{ij} = \sigma_{ij}(Y) - \sigma_{ij}(X) = B_{ijkl}(\eta_X^Y)_{kl} > 0, \quad (7b)$$

for any small perturbative strain (we can assume $\eta_X^Y > 0$ without losing generality). Otherwise, the system becomes unstable. The stability criterion can be cast in terms of the principal minor of the stiffness coefficient,

$$\det |B_{ijkl}| > 0. \quad (7c)$$

This interpretation of the stability criterion is in fact very much in the same spirit as that of the original criterion for the ideal strength of materials proposed by Frenkel [22] and Orowan [23]. We should mention in passing that interpretation of the stability criterion in this way has not been contended seriously despite its simplicity in physical meaning.

As is obvious from the definition, B_{ijkl} does not necessarily retain the symmetry relations of the original crystal since the deformed state Y can be arbitrarily far away from the initial non-deformed state [21]. Given that B_{ijkl} is in general asymmetric while $ij \leftrightarrow kl$, the symmetrized coefficient should be used,

$$\bar{B} = (1/2)(B^T + B). \quad (8)$$

The system becomes unstable when $\det |\bar{B}| = 0$ for the first time under the applied load. In other words, as \bar{B} is a function of the deformation strain, the instability condition will lead to a set of relations among the \bar{B}_{ij} s at the critical applied strain along the primary loading path.

For a cubic crystal subject to hydrostatic pressure P ,

$$\tau_{ij} = -P\delta_{ij}. \quad (9)$$

We follow the convention that the inward pressure is positive while outward stress is negative (i.e., $P < 0$ for tension). From

equations (6) and (9), the elements of the stiffness coefficients are

$$\begin{aligned} B_{11} &= B_{22} = B_{33} = C_{11} - P, \\ B_{12} &= B_{23} = B_{13} = C_{12} + P, \\ B_{44} &= B_{55} = B_{66} = C_{44} - P. \end{aligned} \quad (10)$$

Here we simplify the subscript in the tensor notation by using the Voigt notation ($11 \rightarrow 1$, $22 \rightarrow 2$, $33 \rightarrow 3$, $23 \rightarrow 4$, $31 \rightarrow 5$, and $12 \rightarrow 6$). For this special case, the stiffness coefficients and the elastic constants have the same type of crystal symmetry. And B_{ij} possesses $i \leftrightarrow j$ symmetry, so $\bar{B} = B$. Let $\det |B| \geq 0$; there are three independent stability conditions,

$$B_{11} + 2B_{12} \geq 0, \quad (11)$$

$$B_{11} - B_{12} \geq 0, \quad (12)$$

$$B_{44} \geq 0. \quad (13)$$

Or

$$C_{11} + 2C_{12} + P \geq 0, \quad (14)$$

$$C_{11} - C_{12} - 2P \geq 0, \quad (15)$$

$$C_{44} - P \geq 0, \quad (16)$$

using the elastic constants C_{ij} for the loaded state. The bulk modulus B_T , tetragonal shear modulus G' , and the rhombohedral shear modulus G are defined as follows:

$$B_T = (C_{11} + 2C_{12})/3, \quad (17)$$

$$G' = (C_{11} - C_{12})/2, \quad (18)$$

$$G = 4C_{44}. \quad (19)$$

These quantities are extended to the system under finite hydrostatic load, so we have the corresponding bulk and shear stiffness moduli,

$$B_T(\tau) = (B_{11} + 2B_{12})/3 = (C_{11} + 2C_{12} + P)/3, \quad (20)$$

$$G'(\tau) = (B_{11} - B_{12})/2 = (C_{11} - C_{12} - 2P)/2, \quad (21)$$

$$G(\tau) = 4B_{44} = 4(C_{44} - P). \quad (22)$$

In contrast to the conventional or Born stability criteria only valid in the load-free case, which requires that (17)–(19) be positive, the stability criteria in the system under load require instead (20)–(22) to be positive.

3. Calculation details

3.1. Calculation methods

To simulate hydrostatic deformation, we first calculate the properties (total energy and equilibrium lattice parameter) of a single crystal of Au in the ground state. We performed the *ab initio* DFT calculations using the Vienna *ab initio* simulation package (VASP) [24] developed by the Hafner Research Group at the University of Vienna. VASP uses pseudopotentials or the projector-augmented wave (PAW) method and a plane wave basis set. To obtain a lattice parameter that is in better agreement with the experimental value, we used the

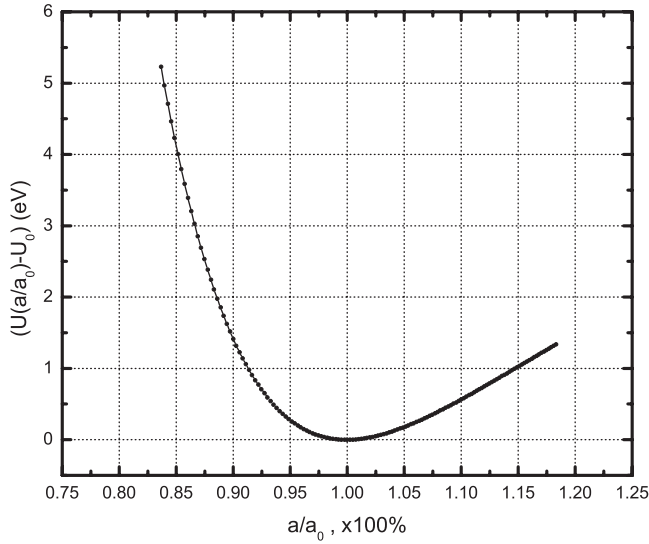


Figure 1. The calculated change of elastic energy versus applied hydrostatic deformation strain. We use a/a_0 as the independent variable.

exchange–correlation energy evaluated with the local density approximation (LDA). Ultrasoft pseudopotentials [25] were always employed to describe the electron–ion interactions. We used an $18 \times 18 \times 18$ k -point mesh in our calculations following the Monkhorst–Pack scheme, which as our experience shows is sufficient for reaching the desired convergence of the total energy and elastic constants. We took the cutoff energy set at $E_{\text{cut-off}}^{\text{Au}} = 292$ eV, which is sufficiently large for the total energy to converge to the stable equilibrium state. For Au, the ground state has a face-centered cubic structure with the lattice parameter $a_0 = 4.07$ Å, which is very close to the experimental measurement 4.08 Å [26] at room temperature. We thus use 4.07 Å as the lattice parameter in our supercell, which is a face-centered cubic cell containing four atoms, to perform the following simulation work for deformation. The benefit of using such a supercell is that we can easily apply specific strains on the supercell and read the values of the six components of the stress tensor directly from VASP output files.

In the next step, we applied hydrostatic deformation to the crystal supercell via a strain, $\eta_{11} = \eta_{22} = \eta_{33} = \xi$, $\eta_{ij} = 0$ for $i \neq j$. We changed the value of ξ from -0.15 to $+0.15$ with a finite step size $\Delta\xi = 0.0025$. This operation amounts to changing the lattice parameter homogeneously. Let a be the lattice constant of the deformed crystal, and obviously $a/a_0 = \sqrt{1 + 2\xi}$ from equations (1) and (2). Applying this type of deformation is equivalent to the application of a hydrostatic stress. We then obtain the internal energy U as a function of the applied strain, or $U = U(a/a_0)$, with the first-principles calculation, as shown in figure 1.

3.2. Elastic energy and stress–strain relations

The elastic energy expanded at each arbitrary deformed configuration when the system changes from state X to state

Y is

$$U(X, \bar{\eta}) = U(X, 0) + V \sum_{ij} \sigma_{ij} \bar{\eta}_{ij} + \left(\frac{1}{2!}\right) V \sum_{ijkl} C_{ijkl} \bar{\eta}_{ij} \bar{\eta}_{kl} + \dots, \quad (23)$$

where $V = a'^3$, $\bar{\eta}$ is a new Lagrangian strain tensor in the deformed configuration X with lattice constant a' . We can simplify the subscript in the tensors by using the Voigt notation. Equation (23) can then be written as

$$V^{-1}[U(X, \bar{\eta}) - U(X, 0)] = \sum_{i=1, \dots, 6} \sigma_i \bar{\eta}_i + \frac{1}{2!} \sum_{i, j=1, \dots, 6} C_{ij} \bar{\eta}_i \bar{\eta}_j + \dots. \quad (24)$$

Considering our face-centered cubic supercell under hydrostatic deformation, given by $\bar{\eta}_1 = \bar{\eta}_2 = \bar{\eta}_3 = \bar{\xi}$, $\bar{\eta}_4 = \bar{\eta}_5 = \bar{\eta}_6 = 0$, plus $\sigma_1 = \sigma_2 = \sigma_3 = \sigma$, we have

$$V^{-1}[U(X, \bar{\eta}) - U(X, 0)] = 3\sigma \bar{\xi} + \left(\frac{3}{2}C_{11} + 3C_{12}\right) \bar{\xi}^2 + \dots. \quad (25)$$

And thus,

$$\sigma = \frac{1}{3V} \left(\frac{\partial U}{\partial \bar{\xi}} \right)_{\bar{\xi}=0}, \quad (26)$$

$$B_T = \frac{C_{11} + 2C_{12}}{3} = \frac{1}{9V} \left(\frac{\partial^2 U}{\partial \bar{\xi}^2} \right)_{\bar{\xi}=0}. \quad (27)$$

So at each deformed configuration with lattice constant a' , we select a few datum points from the U – a/a_0 curve near to a'/a_0 and calculate the strain value $\bar{\xi}$ for each point using X as the reference configuration. Since the elastic energy can be expressed as a polynomial of the strain parameter $\bar{\xi}$ as shown in equations (24) and (25), when we plot the U – $\bar{\xi}$ curve, we may obtain the internal stress (equation (26)) and elastic bulk modulus (equation (27)) through the polynomial fitting mentioned above.

Figure 2 shows the stress calculated in this way. We found that it does agree very well with the Hellmann–Feynman stress calculated by using VASP. As the ideal strength is conventionally defined as the maximum of the stress along the designated deformation path, from figure 2 it appears that the ideal strength for Au is $\sigma_{\text{max}} = -P = 23.45$ GPa at the corresponding hydrostatic strain $a/a_0 = 1.12$. However, we will show below that this is not the true value for the ideal hydrostatic strength, because the stability limit has already been approached before this point via a shear stability bifurcation.

3.3. Elastic constants and elastic stiffness coefficients

As mentioned earlier, there are two ways to calculate elastic stiffness coefficients under load. One is using equation (6), to treat elastic stiffness coefficients as functions of the elastic constants and the applied stress tensor. From equation (27) via fitting of the internal energy, we have the value of $(C_{11} + 2C_{12})/2$ that leads to $B_T(\tau) = (C_{11} + 2C_{12} + P)/3$. So we may test the stability via the so-called volumetric or bulk modulus stability condition (11) or (14), which was also called

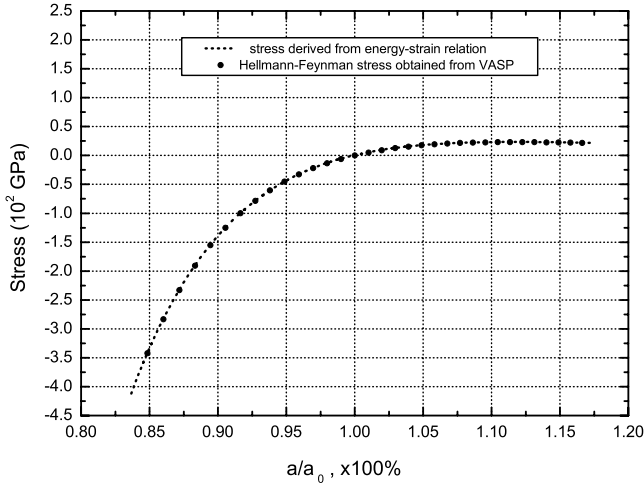


Figure 2. The Hellmann–Feynman stress calculated by using VASP and the stress derived from the energy–strain relation. The maximum stress $\sigma_{\max} = 23.45$ GPa occurs at $a/a_0 = 1.12$.

the mechanical spinodal stability [11]. The other way is using equation (7b), that treats elastic stiffness coefficients as the linear expansion coefficients of the $\delta\sigma-\bar{\xi}$ curve from which one can also get the value of $B_T(\tau)$.

Starting from equations (7), we consider our face-centered cubic supercell under hydrostatic deformation, ($\bar{\eta}_1 = \bar{\eta}_2 = \bar{\eta}_3 = \bar{\xi}$, $\bar{\eta}_4 = \bar{\eta}_5 = \bar{\eta}_6 = 0$, plus $\sigma_1 = \sigma_2 = \sigma_3 = \sigma$). We then have

$$\delta\sigma = (B_{11} + 2B_{12})\bar{\xi} = 3B_T(\tau)\bar{\xi}. \quad (28)$$

So for each deformed configuration with a' as the lattice constant, we take a few points from the $\sigma-a/a_0$ curve (figure 2) close to a'/a_0 , calculate the strain value $\bar{\xi}$ for each point using X as the reference configuration, and then make a linear fitting to equation (28), so we obtain the value of $B_T(\tau)$ at that reference configuration.

As shown in figure 3, this approach arising from the original definition of elastic stiffness coefficients (equations (7)) does give results agreeing with those from the convexity argument of Born and Milstein *et al.* Incidentally, this agreement in our computation provides strong support for the capability and accuracy of the *ab initio* DFT simulation.

3.4. Shear instability and bifurcation away from the hydrostatic strain path

As mentioned in section 1, the stability condition can be violated not through the primary loading path which one intends to examine. For example, in experiments as well as in theory, very often one may find other stability conditions violated before the primary stability condition is, leading to stability bifurcation. Such complications, although abundant in nature and in theoretical scenarios, have not received much attention.

For cubic crystals, two other stability paths are related to shear. To test the two shear stability conditions (12)–(13), we need to give a small perturbative shear strain $\delta\eta$ to each hydrostatically deformed configuration at the given

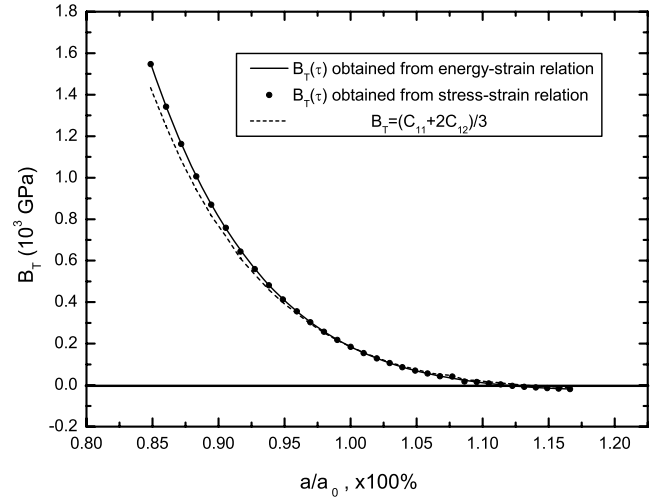


Figure 3. The bulk stiffness modulus is calculated using two approaches. One (smooth line) uses the energy–strain relation, and the other (filled circles) uses the stress–strain relation. The dashed line represents the bulk modulus defined in equation (17).

hydrostatic strain ξ . The strain $\delta\eta$ allows the system to deviate from the main hydrostatic deformation path. Then we check the elastic energy or stress change as a function of $\delta\eta$. With a set of unit lattice vectors (i.e., $[a, 0, 0]$, $[0, a, 0]$, $[0, 0, a]$ in the hydrostatically deformed sample), the perturbative deformation can be described using an appropriate Jacobian matrix J' as

$$r' = J' \cdot r, \quad (29)$$

where r is the position vector corresponding to the current state along the hydrostatic deformation path, and vector r' describes the perturbed state with the shear strain $\delta\eta$.

Under this combined strain state, once again there are two ways to test the stability conditions. The first one is to use the calculated $U-\delta\eta$ curves to obtain the elastic constants through polynomial fitting, which combining with the pressure at this state leads to the (shear) elastic stiffness coefficients. Then we can test whether equation (15) or (16) is violated or not. The second way is to use equations (7). With the given small strain $\delta\eta$, we can obtain the elastic stiffness moduli in the system under load as the linear expansion coefficients from the $\delta\sigma-\delta\eta$ curve, and then check the stability with equations (12) and (13).

The stability condition as presented in equation (12) involves the tetragonal shear modulus, $G' = (C_{11} - C_{12})/2$. Its violation corresponds to a *shear instability*; once it occurs we expect the bifurcation from the hydrostatic deformation path. In order to test this stability condition, we use the following Jacobian matrix (and the corresponding strain matrix for the tetragonal shear) at each point of a'/a_0 along our hydrostatic deformation path:

$$J = \begin{pmatrix} \sqrt{1+2\xi} & 0 & 0 \\ 0 & \sqrt{1-2\xi} & 0 \\ 0 & 0 & 1 \end{pmatrix},$$

$$\delta\eta = \begin{pmatrix} \bar{\xi} & 0 & 0 \\ 0 & -\bar{\xi} & 0 \\ 0 & 0 & 0 \end{pmatrix},$$

Table 1. Zero-pressure elastic stiffness coefficients B_{ij} (in GPa), their pressure derivatives and elastic modulus B_T , G' and G (in GPa).

B_{11}	$\partial B_{11}/\partial P$	B_{12}	$\partial B_{12}/\partial P$	B_{44}	$\partial B_{44}/\partial P$	B_T	G'	G	Reference
202.1	6.34	174.2	5.34	37.9	1.74	183.5	14.0	151.6	This work
201.3	5.97	176.1	5.38	36.9	1.43	184.5	12.6	147.6	[27]
192.2	7.01	162.8	6.14	42.0	1.79	172.6	14.7	168.0	[28] (RT)
192.9	5.71	163.8	4.95	41.5	1.52	167.2	14.6	166.0	[29] (RT)
200.4	6.49	169.5	5.66	44.5	1.79	179.8	15.5	178.0	[30] (79 K)

where $\bar{\xi}$ is the magnitude of the shear strain. With such increments of the tetragonal deformation, the energy of the system changes according to the relation (24),

$$\delta U = V(C_{11} - C_{12})\bar{\xi}^2 + \dots, \quad (30)$$

where $V = a^3$ is the current volume. The tetragonal shear modulus $G' = (C_{11} - C_{12})/2$ can be expressed as

$$G' = \frac{1}{4V} \frac{\partial^2 U}{\partial \bar{\xi}^2}. \quad (31)$$

And then,

$$G'(\tau) = G' - P. \quad (32)$$

Or if we use a second approach employing the stress-strain relation with equations (7), we have

$$\delta \sigma_1 = (B_{11} - B_{12})\bar{\xi} = 2G'(\tau)\bar{\xi}, \quad (33)$$

and then we have

$$G'(\tau) = \frac{1}{2} \frac{\partial \sigma_1}{\partial \bar{\xi}}. \quad (34)$$

The second shear stability corresponding to the condition in equation (13) is the rhombohedral shear instability, $G(\tau) = 4(C_{44} - P)$. To explore the bifurcation along the rhombohedral shear strain, we used the following perturbative shear strain matrix:

$$\delta \eta = \begin{pmatrix} 0 & 0 & 0 \\ 0 & 0 & \bar{\xi} \\ 0 & \bar{\xi} & 0 \end{pmatrix}.$$

The corresponding elastic energy change now becomes

$$\delta U = 2V\sigma_4\bar{\xi} + 2VC_{44}\bar{\xi}^2 + \dots, \quad (35)$$

and the elastic constants are

$$C_{44} = \frac{1}{4V} \frac{\partial^2 U}{\partial \bar{\xi}^2}, \quad (36)$$

$$G(\tau) = \frac{1}{V} \frac{\partial^2 U}{\partial \bar{\xi}^2} - 4P. \quad (37)$$

Alternatively, from the stress-strain relation (equations (7)), we have

$$\delta \sigma_4 = 2B_{44}\bar{\xi}, \quad (38)$$

$$G(\tau) = 2(\partial \sigma_4 / \partial \bar{\xi}). \quad (39)$$

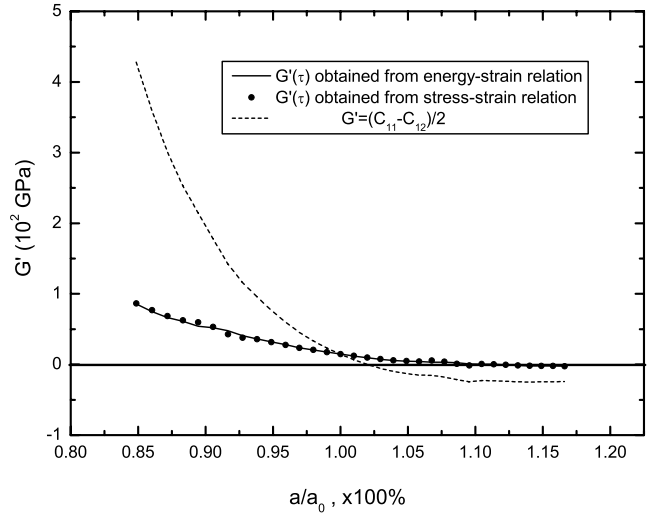


Figure 4. The tetragonal shear stiffness modulus calculated using two approaches. One (smooth line) is using the energy-strain relation, and the other (filled circles) is using the stress-strain relation. The dashed line represents the modulus defined in equation (18).

4. Results

Table 1 summarizes the elastic stiffness coefficients B_{11} , B_{12} , B_{44} and their derivatives with respect to pressure calculated in this work using DFT. The zero-pressure values of the B_{ij} s obtained agree well with the previous theoretical calculations using the *ab initio* full-potential linear muffin-tin orbital (FP-LMTO) method [27]. Our results show better agreement with low-temperature experimental data than the room temperature data [28–30]. Under compression, Au exhibits stability over the entire range of applied strain (strain up to $a/a_0 = 0.83$ and pressure up to 412 GPa). Under expansion, Au exhibits much complex stability behavior which is presented below.

The bulk stiffness modulus $B_T(\tau)$ obtained from the two different approaches, one from the $U-\bar{\xi}$ relation and the other from the $\sigma-\bar{\xi}$ relation, are nearly identical, and so are the shear stiffness moduli $G'(\tau)$ and $G(\tau)$ as shown in figures 3–5. Figure 3 shows that the hydrostatic or volume strain stability condition (equation (11)) is violated at the point $a/a_0 = 1.12$ where the bulk modulus vanishes. B_T and $B_T(\tau)$ reach zero at almost the same strain, $a/a_0 = 1.12$. On the other hand, the tetragonal shear stability condition (equation (12)) is not violated until $a/a_0 = 1.09$ as shown in figure 4. Looking at the rhombohedral shear stability condition (equation (13)), we see that the rhombohedral shear stiffness modulus $G(\tau)$ disappears at a much smaller value of $a/a_0 = 1.06$ as shown in figure 5. So our *ab initio* calculations gave the following

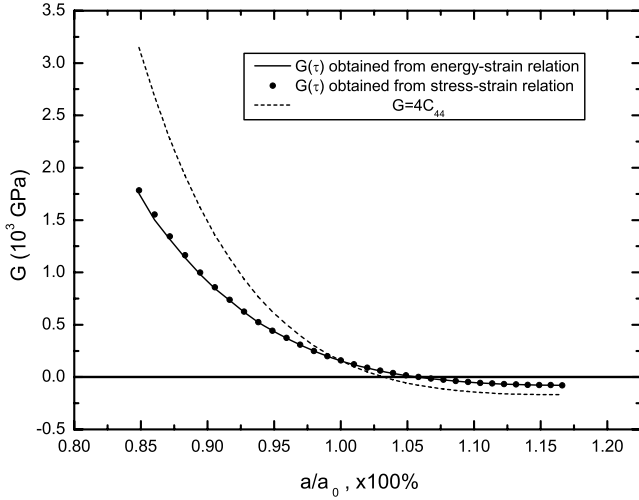


Figure 5. The rhombohedral shear stiffness modulus calculated using two approaches. One (smooth line) is using the energy–strain relation, and the other (filled circles) is using the stress–strain relation. The dashed line represents the modulus defined in equation (19).

sequence in terms of applied hydrostatic strains where the corresponding instability conditions are violated for Au under hydrostatic expansion: the rhombohedral shear stability limit is reached at $a/a_0 = 1.06$, the tetragonal shear stability limit at $a/a_0 = 1.09$, and the hydrostatic stability limit at $a/a_0 = 1.12$. According to the stability criterion, the system should become unstable at the smallest value of the applied strain that corresponds to the first violation of the stability conditions. For Au subject to hydrostatic expansion, therefore, we show that it is at $a/a_0 = 1.06$, and the instability is dominated by rhombohedral shear. The corresponding ideal strength of Au under hydrostatic expansion is found to be 19.2 GPa.

As mentioned in section 1, the instability for systems like Au was expected to occur along the primary loading path of hydrostatic expansion [11]. However, our results show that the occurrence of the shear instability at $a/a_0 = 1.06$ precedes and intervenes in the volumetric instability that occurs at $a/a_0 = 1.12$. This preemptive effect clearly represents a stability bifurcation deviating from the primary loading path. To illustrate this point further, we plot the shear stress–strain relation in figure 6 for the system subject to the rhombohedral shear strain η_4 at the given hydrostatic expansion. The stress–strain relation shows that, when $a/a_0 < 1.06$, the slope of this σ_4 – $\eta_4/2$ curve at the initial point is positive, i.e. $B_{44} > 0$; when $a/a_0 \geq 1.06$, the slope becomes negative, i.e. $B_{44} \leq 0$. As shown in figure 2, the slope of the volumetric stress–strain curve along the hydrostatic strain direction, or the bulk stiffness constant B_T , is still positive at $a/a_0 = 1.06$, and only becomes zero at $a/a_0 = 1.12$. Note that the negative stress–strain relation at small strain, which corresponds to an unstable state, is predicted from the calculation when the finite strain is imposed on the system. In reality, of course, such a scenario may not be seen, as a possible change of structure could occur precipitously.

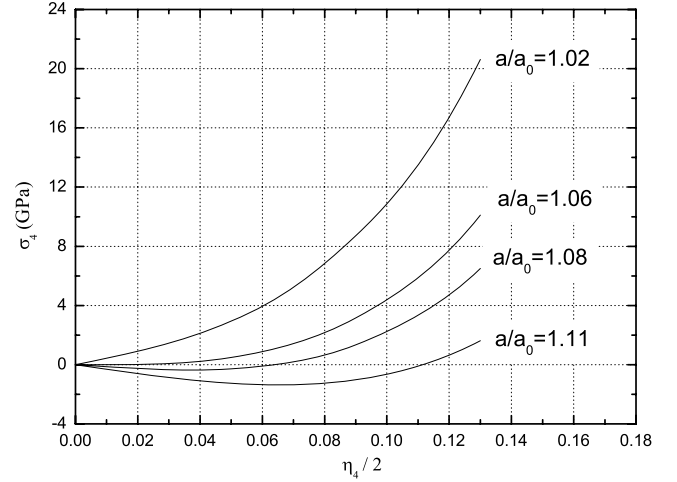


Figure 6. At each configuration with hydrostatic expansion, we give a perturbation of the rhombohedral shear strain η_4 and calculate the stress–strain relation for the system. The slope of the curve involves the rhombohedral shear stiffness modulus B_{44} which becomes negative at $a/a_0 \sim 1.06$.

5. Discussion

The stability limits for Au were investigated earlier by Wang *et al* using classical molecular dynamics simulation [11]. In their work, the bulk stiffness modulus disappears first with volume expansion at around $a/a_0 = 1.06$, which was followed by void formation. The tetragonal shear stiffness modulus remains larger than zero until $a/a_0 = 1.09$ and the rhombohedral shear stiffness modulus is nonzero until $a/a_0 = 1.08$. The results led them to conclude that the instability is caused by volumetric instability, or along the primary loading path. The difference between the MD and the current DFT calculation could originate from several causes. Firstly, since a semi-empirical inter-atomic potential was used in the MD simulation, certain differences should be expected as compared with *ab initio* calculations, especially when dealing with large deformation strains (6–12%) which may not be adequately considered when fitting the potential. Secondly, since the MD work was performed at elevated temperatures (200–1200 K), one would expect the elastic constants as well as the elastic stiffness constants to be different. Consequently, the softening of these constants at high temperature should lead to smaller critical strains corresponding to the instability points (equations (12) and (13)) than those at zero temperature as seen in our DFT calculation. However, as it is known that the bulk modulus decrease versus temperature rise is in general much slower than the shear moduli for most metals including Au [30], one would still expect to see shear instability intervene before the volumetric instability, as the shear moduli are already much smaller than the bulk modulus in the first place. Thirdly, the stability limits in the MD results were obtained from extrapolations from the datum points away from the critical points, as it is known that the increasing thermal fluctuation makes the MD simulation less reliable close to those points [31]. In contrast, in the DFT calculation, we can push the calculation very close to and even beyond the

instability points. Finally, it is worth noting that the small sample size used in the DFT calculation may limit the void formation which was identified as the hallmark of instability in the MD work. But this limitation is irrelevant in the elastic stability modeling since we are only focusing on approaching the stability limit from one side of the phase, not on how the new phase (i.e. void) forms.

Besides these technical reasons, we believe that some of these differences are rooted in the fundamental interpretation of structure or lattice stability. As pioneered by Born, the elastic instability of a lattice is governed by the vanishing of the convexity of the elastic energy as a function of varying strain. The first application of this theory was to melting of crystals [2, 3] where vanishing of the shear modulus at the onset of liquid phase formation was thought to be a direct indication of the elastic instability. Under applied stress, Born's convexity argument should still hold but with a few modifications given by Hill and Milstein [4, 5]. As argued by Born and later Hill, the presence of many fluctuations and secondary processes accompanying the primary deformation strain, including sample loading conditions and rotations, could lead to instabilities different from that expected from the primary deformation path. In the hydrostatic expansion of Au, as we clearly demonstrated, it is the shear instability that precedes the volume or bulk instability. This bifurcation process, as we identified here, must be treated carefully when identifying the instability points and subsequently the formation of new structures or defects.

Moreover, we should note that the bifurcation observed along the rhombohedral shear direction simply tells us that the atoms in the system at the instability point are going to be engaged in displacement along the rhombohedral shear directions, thus breaking the original crystal symmetry. For the same reason, the atomic displacement is not necessarily correlated, but rather random. This leads to local symmetry breaking that precedes the local volume expansion, eventually resulting in void formation. In other words, the so-called volumetric instability with void formation may be initiated or nucleated by the shear deformation. In order to test this mechanism directly, one may need to use a system with minimum dimension larger than the critical nucleation size of the void.

The calculations that we performed focus mostly on the long-wavelength phonon limit and zero temperature. It is possible that, before violating the rhombohedral shear stability condition, some soft phonon modes or other instabilities may appear in the hydrostatically deformed crystal. Actually recent studies on elastic [18] and phonon [32] instabilities of aluminum support the suggestion that this may happen in fcc metals. On a more fundamental level the elastic stability of a crystal needs to be investigated in terms of electronic structure. Such a scenario for Au will be explored in the future.

6. Conclusion

In this work, we first identified the elastic stiffness constant as the coefficient of the stress-strain relation in an arbitrary deformed state. And then we used it to explain the stability

criterion. This type of interpretation is what Frenkel and Orowan originally proposed for judging the stability limit for solids. Using an *ab initio* calculation, we explored the elastic stability in terms of the relations between the internal energy, stress, and strains in Au subject to hydrostatic stress (tension and compression). More importantly, we introduced perturbations along non-primary loading directions. We show from the results that the stability limit of Au under a hydrostatic load is governed by the rhombohedral shear perturbation-induced instability, not by volumetric instability which occurs at a delayed critical volume strain. The preemptive shear instability represents a bifurcation of the crystal instability away from the primary loading path, as originally considered by Born and Hill.

Acknowledgments

The authors are grateful for the financial support of this work provided by the US Army Research Office (ARO) under the contract number ARO-W911NF-07-1-0490 and DARPA SAM II through ONR under the contract number N00014-06-1-0490.

References

- [1] Van Vliet K J *et al* 2003 *Phys. Rev. B* **67** 15
- [2] Born M 1940 *Proc. Camb. Phil. Soc.* **36** 160
- [3] Born M and Huang K 1956 *Dynamical Theory of Crystal Lattices* (Oxford: Clarendon)
- [4] Hill R 1975 *Math. Proc. Camb. Phil. Soc.* **77** 225
- [5] Hill R and Milstein F 1977 *Phys. Rev. B* **15** 3087
- [6] Milstein F and Hill R 1977 *J. Mech. Phys. Solids* **25** 457
- [7] Milstein F and Hill R 1978 *J. Mech. Phys. Solids* **26** 213
- [8] Milstein F and Hill R 1979 *J. Mech. Phys. Solids* **27** 255
- [9] Milstein F 1982 *Mechanics of Solids* (Oxford: Pergamon)
- [10] Wang J H *et al* 1993 *Phys. Rev. Lett.* **71** 4182
- [11] Wang J H *et al* 1995 *Phys. Rev. B* **52** 12627
- [12] Zhou Z and Joos B 1996 *Phys. Rev. B* **54** 3841
- [13] Morris J W and Krenn C R 2000 *Phil. Mag. A* **80** 2827
- [14] Djohari H, Milstein F and Maroudas D 2007 *Appl. Phys. Lett.* **90** 161910
- [15] Senoo M, Fujishiro I and Hirano M 1984 *Bull. JSME—Japan Soc. Mech. Eng.* **27** 2680
- [16] Esposito E *et al* 1980 *Phil. Mag. A* **41** 251
- [17] Friak M, Sob M and Vitek V 2003 *Phil. Mag. A* **83** 3529
- [18] Li W X and Wang T C 1998 *J. Phys.: Condens. Matter* **10** 9889
- [19] Černý M *et al* 2004 *J. Phys.: Condens. Matter* **16** 1045
- [20] Černý M 2007 *Mater. Sci. Eng. a* **462** 432
- [21] Wallace D C 1998 *Thermodynamics of Crystals* (New York: Dover)
- [22] Frenkel J 1926 *Z. Phys.* **37** 572
- [23] Orowan E 1949 *Rep. Prog. Phys.* **12**
- [24] Kresse G and Furthmüller J 1996 *Phys. Rev. B* **54** 11169
- [25] Vanderbilt D 1990 *Phys. Rev. B* **41** 7892
- [26] *American Institute of Physics Handbook* 1970 (New York: McGraw-Hill)
- [27] Tsuchiya T and Kawamura K 2002 *J. Chem. Phys.* **116** 2121
- [28] Daniels W B and Smith C S 1958 *Phys. Rev.* **111** 713
- [29] Hiki Y and Granato A V 1966 *Phys. Rev.* **144** 411
- [30] Biswas S N, Vantklooster P and Trappeniers N J 1981 *Physica B & C* **103** 235
- [31] Ray J R 1988 *Comput. Phys. Rep.* **8** 109
- [32] Clatterbuck D M *et al* 2003 *Phys. Rev. Lett.* **91** 135501